ResearchGate

See discussions, stats, and author profiles for this publication at: https://www.researchgate.net/publication/279547121

Skin Detection in Hyperspectral Images

Conference Paper · April 2015

DOI: 10.1117/12.2179332

CITATIONS
0

READS
185

2 authors, including:

Miguel Velez-Reyes
University of Texas at El Paso
197 PUBLICATIONS **1,621** CITATIONS

SEE PROFILE

Some of the authors of this publication are also working on these related projects:

Advanced Unmixing of Hyperspectral Remote Sensing Data for Space Situational Awareness View project

NOAA-Cooperative Science Center for Earth System Sciences and REmote Sensing Technologies (NOAA-CREST) View project

All content following this page was uploaded by Miguel Velez-Reyes on 03 July 2015.

The user has requested enhancement of the downloaded file.

Skin Detection in Hyperspectral Images

Stephanie Michelle Sanchez, Miguel Velez-Reyes
Department of Electrical and Computer Engineering
The University of Texas at El Paso,
500 W University Avenue, El Paso, TX 79968, USA
Ph. 1.915.747.5470, Fax 1.915.747.7871
E-mail: mvelezreyes@utep.edu, sanchez.engenheiro@gmail.com

ABSTRACT

Hyperspectral imagers collect information of the scene being imaged at close contiguous bands in the electromagnetic spectrum at high spectral resolutions. The number of applications for these imagers has grown over the years as they are now used in various fields. Many algorithms are described in the literature for skin detection in color imagery. However increased detection accuracy, in particularly over cluttered backgrounds, and of small targets and in low spatial resolution systems can be achieved by taking advantage of the spectral information that can be collected with multi/hyperspectral imagers. The ultimate goal of our research work is the development of a human presence detection system over different backgrounds using hyperspectral imaging in the 400-1000nm region of the spectrum that can be used in the context of search and rescue operations, and surveillance in defense and security applications. The 400-1000 nm region is chosen because of availability of low cost imagers in this region of the spectrum. This paper presents preliminary results in the use of combinations of normalized difference indices that can be used to detect regions of interest in a scene that can be used as a pre-processor in a human detection system. A new normalized difference ratio, the Skin Normalized Difference Index (SNDI) is proposed. Experimental results show that a combination the NDGRI+NDVI+SNDI results in a probability of detection similar to that of the NDGRI. However, the combination of features results in a much lower probability of false alarm.

Keywords: hyperspectral image processing, skin detection, normalized difference index,

1. INTRODUCTION

Many algorithms are described in the literature for human skin detection in color imagery [1]. However increased detection accuracy, in particularly over cluttered backgrounds, and of small targets and in low spatial resolution systems can be achieved by taking advantage of the spectral information that can be collected with multi/hyperspectral imagers.

The ultimate goal of our research work is the development of a human presence detection system over different backgrounds using hyperspectral imaging in the 400-1000 nm region of the electromagnetic spectrum. Such as system can be an important component in search and rescue operations, and surveillance applications in defense and security. The 400-1000 nm region is chosen because of availability of low cost hyperspectral imagers in this region of the spectrum from multiple vendors.

In this paper, we present experimental results comparing the performance of different normalized different indices (NDI) for skin detection. Due to their simplicity and robustness, NDI are attractive features to use in the pre-screening stage of a target detection system to identify regions of interest that can be further studied using more standard target detection techniques for identification.

2. BACKGROUND

2.1 Hyperspectral Imaging

Hyperspectral imaging (HSI) is a technology that provides fully registered spatial and high-resolution spectral (radiance, reflectance, or emission) information of the scene in the field of view of the sensor [2]. Hyperspectral imagers have hundreds of narrow contiguous bands. Hyperspectral imagers utilize reflected light or emitted light as the energy source. The illuminating source must provide a broadband source to ensure all wavelengths in the sensor's spectral range are

Algorithms and Technologies for Multispectral, Hyperspectral, and Ultraspectral Imagery XXI,
edited by Miguel Velez-Reyes, Fred A. Kruse, Proc. of SPIE Vol. 9472, 94721P
© 2015 SPIE · CCC code: 0277-786X/15/$18 · doi: 10.1117/12.2179332

Downloaded From: http://proceedings.spiedigitallibrary.org/ on 05/30/2015 Terms of Use: http://spiedl.org/terms

energized. Under proper illumination conditions these imagers may be used to identify and characterize certain scene features based on spectral signatures.

2.2 Skin Spectra

Figure 1 shows examples of typical skin reflectance signatures for different percentages of melanosomes. Skin reflectance is mainly determined, particularly in the visible region of the spectrum, by the chromophores (melanin, keratin, carotene, collagen and hemoglobin) present in the various layers of the skin. For the signatures in Fig. 1, Skin with less melanin appears brighter because it has higher reflectance. Human skin spectral signature exhibits numerous distinctive features (e.g. absorption features) in the visible and NIR regions of the electromagnetic spectrum that can be exploited for skin detection over cluttered backgrounds [3, 4, 5]. For instance, human skin is more red than green which can be used to discriminate skin from green vegetation (more green than red). Note also the absorption feature around 980 nm and the general behavior of skin reflectance above 1000 nm. The normalized difference indices described later take advantage of these features.

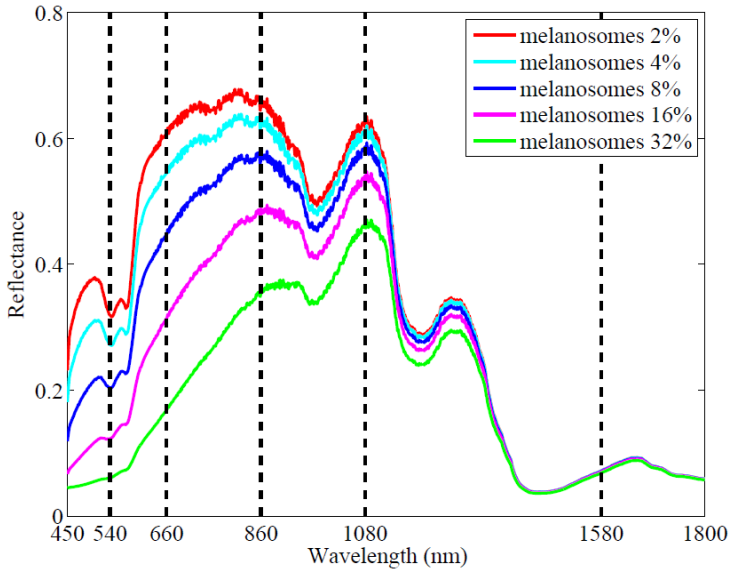

Figure 1. Spectral reflectance of human skin at VIS-SWIR wavelengths (from [3]).

2.3 Skin Detection using Color Imaging

Many algorithms are described in the literature for skin detection in color imagery, see [1] for a review. Skin detection approaches using color imagery are based on features derived from different color space representations (e.g. RGB, normalized RGB, YCrCb). The main advantage to these methods is that they are simple and easy to implement based on the desired classification rules. Some of the obstacles or limitations that one may face when utilizing these techniques are the high occurrence of false alarms particularly in cluttered environments. Evidently false alarms are inevitable in most real world scenarios since any object that has a color similar to skin will be classified as skin. In addition, detection accuracy varies with the lighting conditions and the melanosomes percentage on the individual.

2.4 Skin Detection using Hyperspectral Imaging

Skin detection using hyperspectral imaging has been a recent growing field in security and defense. Some examples are described here. In [6], rescue robots used hyperspectral imaging to locate victims after a natural disaster (i.e. earthquake). Their findings showed that skin can be detected using hyperspectral imaging even after a body is covered by debris (i.e. ash). Also, their results indicated that hyperspectral imaging analysis provided a much higher skin detection accuracy rates than detection using color and thermal imaging.

Hyperspectral imaging was used for monitoring and evaluation of skin pigmentations in [7]. Using the spectral information, they were able to estimate the volume fraction of melanosomes, volume fraction of blood, hemoglobin oxygen saturation, along with other skin parameters. Their results compared well with published values for these quantities.

Downloaded From: http://proceedings.spiedigitallibrary.org/ on 05/30/2015 Terms of Use: http://spiedl.org/terms

In [4, 8], normalized difference indices that take advantage of skin spectral features were proposed in order to detect skin. Their proposed approach significantly reduced the number of false alarms attributed to human-like objects.

3. METHODOLOGY

The overall goal of this project was to study different combinations of features that will facilitate detection of skin over multiple backgrounds. The flowchart in Figure 2 provides an overview of the experimental methodology. In this work, we examined collected hyperspectral images of people over different backgrounds and studied combinations of different normalized difference ratios as feature candidates. The multispectral ratios are organized into an image cube format that is processed using the Hyperspectral Image Analysis Toolbox (HIAT) [9]. In HIAT, classes as well as testing and training sets are visually identified. After the testing and training sets are selected, the Euclidean distance classifier is applied to the image. Classification accuracy results are used as a proxy to determine how well different feature combinations help discriminate between skin and non-skin classes.

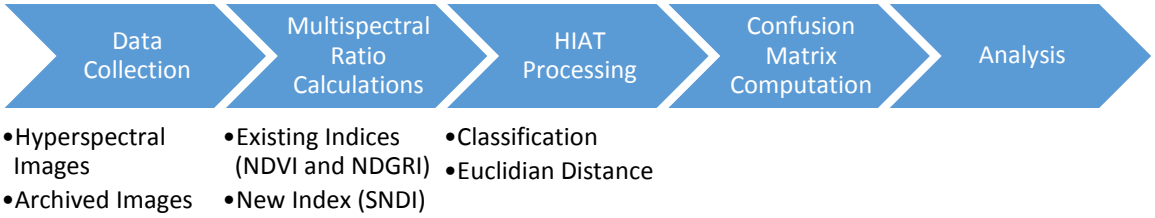

Figure 2. Summary of the experimental methodology.

Some of the hyperspectral images utilized in this research were collected using a Surface Optics' SOC710-VP Hyperspectral Imager. The specifications of this imager are given in Table 1. Notice that the spectral coverage of the imager is between 400-100nm. This was an important restriction as it is of interest in our work to perform detection using imagers in that spectral range where systems are of significantly lower cost than systems in the NIR where skin detection is easier to detect. Archived data collected with imagers of similar characteristics from collaborators was also used.

Table 1. SOC710-VP Hyperspectral Imager Specifications.

Spectral Coverage:	400-1000 nanometers
Spectral Resolution:	4.6875 nanometer
Bands:	128
Dynamic Range:	12-bit
Pixels per line:	696
Speed:	30 spatial lines per second, 23.2 seconds/cube (696 by 520 cube)
Focal Length:	Configurable (based on lens used)
Lens Type:	C-Mount
Weight:	2.95 Kg (6.5 lbs.)
Dimensions (HWL):	9.5 x 16.8 x 22cm (3.75 x 6.62 x 8.66 in.)
Power:	12-VDC / 100-240VAC (50-60Hz)

2.1 Multispectral Normalized Difference Ratios

Band ratios and normalized indices are commonly used in multi/hyperspectral image analysis [10]. Our ultimate goal is to develop a system that can detect human skin over different backgrounds that can be used as part of a search and rescue system, or in defense and security applications (e.g. sniper and dismount detections). Normalized indices are simple to compute and can be used as part of a pre-processing stage to detect regions of interest and reduce the dimensionality of the search space. Normalized difference indices are often used for detection as they are invariant to offset and scaling that occur due to transitivity and scattering. We look at combinations that include indices that highlight background (e.g. vegetation) and those that highlight skin.

A common normalized index used in remote sensing is the Normalized Difference Vegetation Index (NDVI) [10]

Downloaded From: http://proceedings.spiedigitallibrary.org/ on 05/30/2015 Terms of Use: http://spiedl.org/terms

$$NDVI = \frac{\rho_{NIR} - \rho_{red}}{\rho_{NIR} + \rho_{red}}, \quad (1)$$

NDVI has been used in remote sensing to assess whether the target being observed contains live green vegetation or not. It takes advantage of the red edge feature present in vegetation spectra. The reader is referenced to (Schowengerdt, 2007) for further details.

Normalized difference indices have been proposed as features for skin detection. In (Nunez et al., 2008; Nunez, 2010), the Normalized Difference Skin Index (NDGRI) and the Normalized Difference Green-Red Index (NDGRI) were proposed as computationally simple features that can provide high probability of detection with low probability of false alarm. The NDSI is a function of reflectance at 1080nm and 1580nm. The reflectance at 1080nm is the location of a local maximum (see Fig. 1) of the reflectance of skin in the NIR where melanosome absorption dominates. A stable yet low-valued reflectance feature in skin spectra is chosen at 1580nm, in order to ensure a large difference between melanin-dominated and water-dominated portions of the skin spectra. The NDSI is given by [3, 4, 8],

$$NDSI = \frac{\rho_{1080} - \rho_{1580}}{\rho_{1080} + \rho_{1580}}, \quad (2)$$

The color green comprises of the 495nm through 570nm region of the spectra while green color ranges from 620nm through 750nm. As Fig. 1 shows, human skin is more red than green while vegetation is more green than red. The NDGRI is given by [3, 4, 8],

$$NDGRI = \frac{\rho_{green} - \rho_{red}}{\rho_{green} + \rho_{red}} \quad (3)$$

Human skin will result in negative values of NDGRI while vegetation will result in positive value. Clearly these differences can be used to discriminate between skin over a vegetation background. In (1)-(3), ρ_{NIR}, ρ_{red}, and ρ_{green} are the reflectance values of near-infrared, red, and green. In our experiments, the NIR wavelength value was set at 860 nm, the red at 650 nm, and the green at 510 nm. The results of [3, 4, 8] were very encouraging but the requirements of a hyperspectral imager covering the VIS and NIR ranges (400nm to 1700 nm) presents a cost challenge for implementation.

In this work, we limited our focus to imager in the 400 nm to 1000 nm. Cost of imagers in this spectral range is 4 to 5 times lower than those covering up to 1800 nm. Hence we will not use the NDSI in (1), An interesting spectral feature not explored in [3, 4, 8] is the spectral difference between the skin reflectance peak around 800 nm and the absorption feature around 980 nm. Based on this feature, we propose the Skin Normalized Difference Index (SNDI)

$$SNDI = \frac{\rho_{980} - \rho_{800}}{\rho_{980} + \rho_{800}} \quad (4)$$

A weakness of this feature compared to the NDSI is that and the percentage of melanosomes increase the difference becomes smaller.

Table 2. Feature Combinations studied in the experiments.

Image Label	Feature Combinations
One	All spectral bands
Two	NDGRI, NDVI, SNDI
Three	NDGRI, SNDI
Four	NDGRI,SNDI
Five	NDVI, SNDI
Six	NDGRI
Seven	SNDI

Downloaded From: http://proceedings.spiedigitallibrary.org/ on 05/30/2015 Terms of Use: http://spiedl.org/terms

2.2 Feature combinations

Six feature cubes were created using multiple ratio combinations. Table 2 shows the different feature combinations cubes analyzed using HIAT. NDVI was not studied by itself as it is a vegetation index ratio not designed for skin detection.2.3 Hyperspectral Image Analysis Toolbox (HIAT)

HIAT is a Matlab toolbox developed at the University of Puerto Rico – Mayaguez (UPRM) [9]. It is a computational environment that contains hyperspectral image processing algorithms developed at the UPRM Laboratory for Applied Remote Sensing and Image Processing (LARSIP). Some of the features this toolbox contains are image enhancement, band subset section, unmixing, feature extraction, supervised classification, and unsupervised classification. Many of these features can be applied to multi-feature imaged organized in a cube format not only to hyperspectral imagery.

2.4 Classification Analysis

HIAT was used to conduct the classification analysis. Testing and training sets were selected for each image through visual examination. The supervised training and testing sets were created by selecting areas using polygons in the images and labeling them with the corresponding class as shown in Fig. 3. The same testing and training polygons and labels were utilized for all of the feature combinations for a given image. After the testing and training sets were created, the Euclidean distance classifier was applied to all feature cubes. Classification accuracies were used as proxies for discrimination power of the selected features.

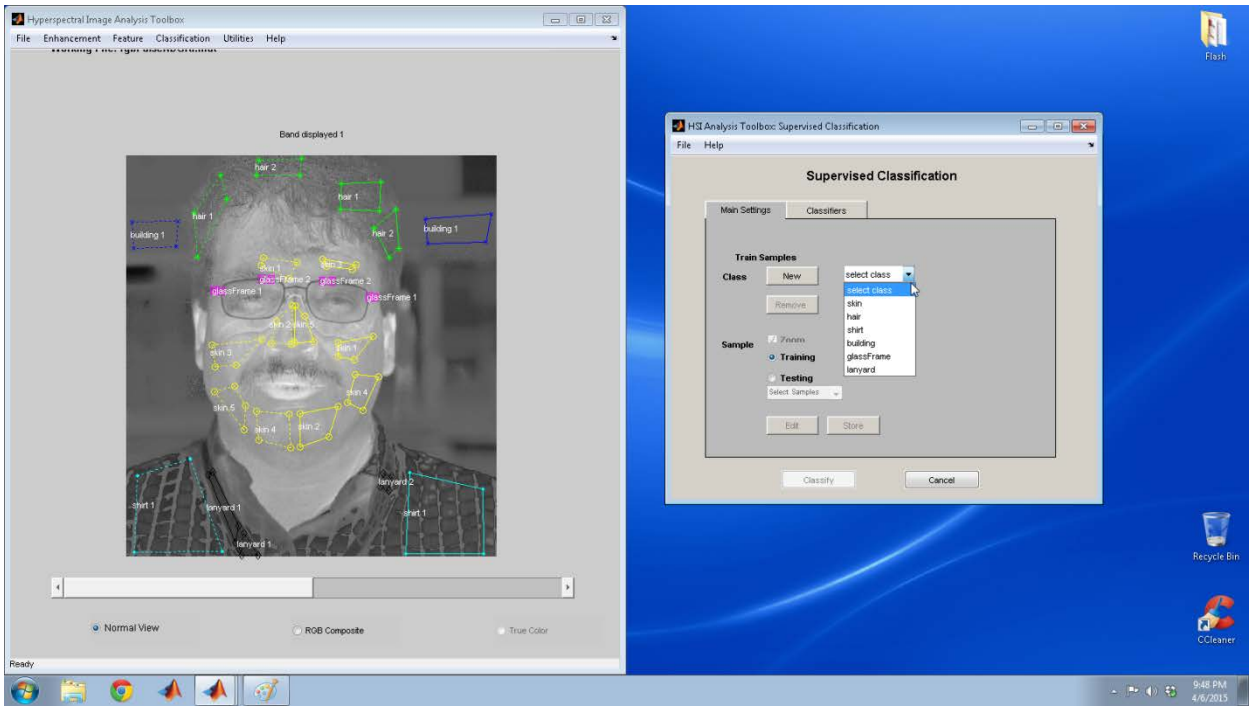

Figure 3. Testing and training pixels selection using HIAT.

2.5 Euclidean Distance Classification

The Euclidean distance classifier is a simple classification rule where the pixel under evaluation is assigned to the class whose mean is the closest to the sample under evaluation. See reference [10, 11] for more details.

Downloaded From: http://proceedings.spiedigitallibrary.org/ on 05/30/2015 Terms of Use: http://spiedl.org/terms

2.6 Accuracy Assessment

Contingency tables, also known as confusion matrices, are used to assess the accuracy of the classification result. To facilitate the accuracy analysis, the results for all the non-skin classes in the image are lumped together into a single "non-skin" class. The resulting confusion matrix is a 2x2 matrix shown in Table 3.

This table is created utilizing the reference (user) data and the classified (producer) data. The reference refers to the number of times an event occurred, while the producer refers to the number of times an event was forecasted. A hit refers to the instances where an event occurrence was forecasted. A false alarm refers to the instances where an event was forecasted but did not occur. A miss refers to the instances where an event occurred but was not forecasted. A null event refers to the instances where an event did not occur and was not forecasted. Table 3 shows how all of these events are arranged in a confusion matrix [11].

After an image is collected and the contingency table is created, the user, producer, and total accuracy percentages are calculated. Table 3 shows how these values are computed for the 2x2 contingency table. The producer's accuracy is an estimate of the probability that the classifier has labeled an image pixel into Class A given that the ground truth is Class A, while the user accuracy describes the probability that a pixel is Class A given that the classifier has labeled the pixel into Class A [11].

Table 3. Simplified Contingency Table and Accuracy Assessment.

		Field Verified Density Class		
		Skin	Non-Skin	User's Accuracy
Interpreted Density Class	Skin	I	II	$\frac{I}{I+II}$
	Non-Skin	III	IV	$\frac{IV}{III+IV}$
	Producer's Accuracy	$\frac{I}{I+III}$	$\frac{IV}{II+IV}$	Total Accuracy $\frac{I+IV}{I+II+III+IV}$

4. RESULTS AND DISCUSSION

Sample results on a face image (Subject-1) in front of a building and an image of a person in front of vegetation background (Subject-4) are presented here. Figure 4 (a)-(c) shows the results of a color palette applied to each of the ratio images for the face image of Subject-1. Figure 4(d) shows a false RGB composite where NDGRI is in the red band, NDVI is in the green band and SNDI is in the blue band.

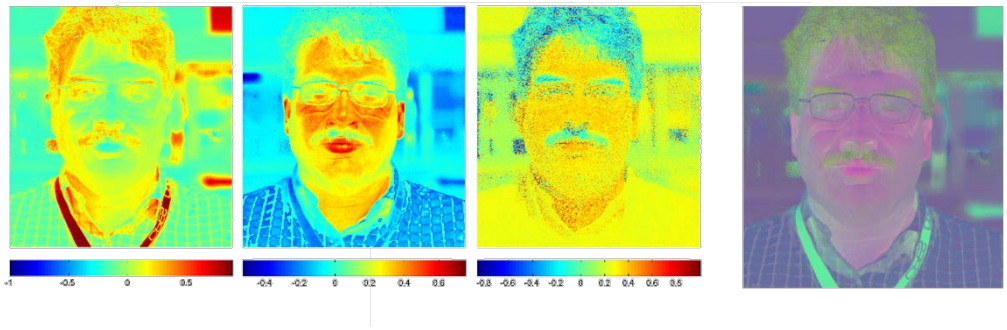

(a) (b) (c) (d)

Figure 4. Color palettes for (a) NDVI, (b) NDGRI (c) SNDI and (d) RGB composite using R-NDGRI, G-NDVI and B-SNDI.

Downloaded From: http://proceedings.spiedigitallibrary.org/ on 05/30/2015 Terms of Use: http://spiedl.org/terms

The face is clearly highlighted in Fig. 4(b) and Fig. 4(c) for NDGRI and SNDI respectively. The face in not highlighted in NDVI in Fig. 4(a) and there is no reason to believe it will be since NDVI is designed for vegetation. Notice that NDGRI is also capable of detecting the face of a person in the background next to the left ear of Subject-1. Visual assessment suggests that NDGRI produces the best discrimination between skin and non-skin. In the RGB composite, the face of Subject-1 and the skin of the person in the background are shown in a pinkish color tone.

Classification results for all feature images in Table 2 using the training and testing samples shown in Figure 3 are shown in Figure 5 for Subject-1. In the binary images, the white color represents the skin class and the black is the non-skin class.

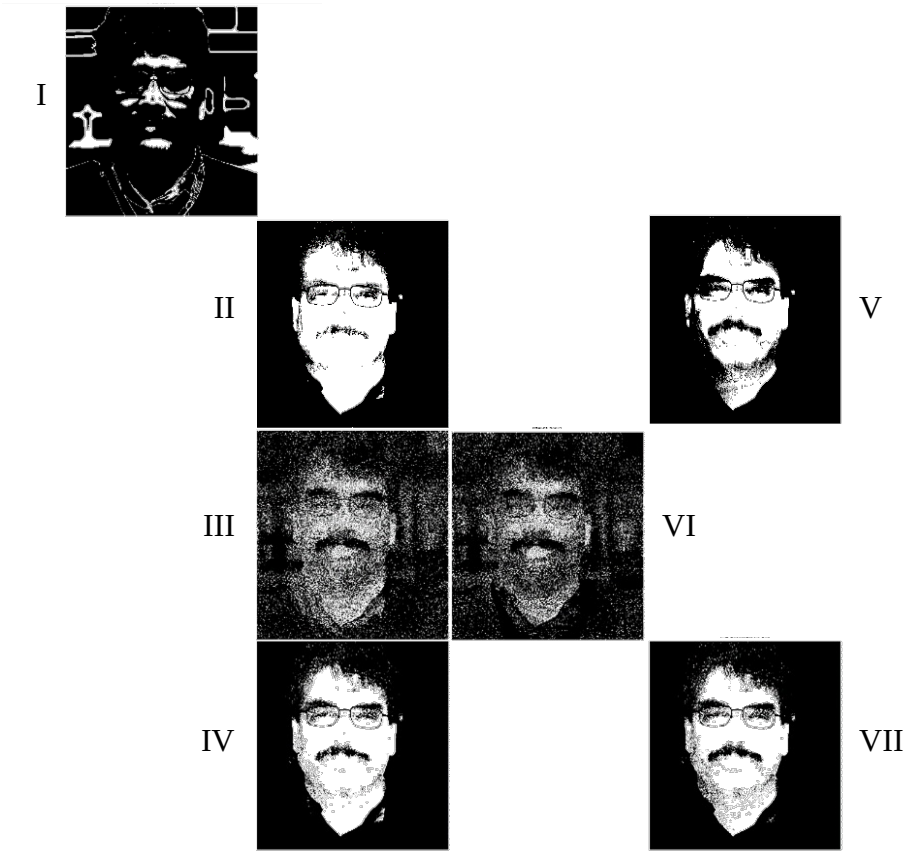

Figure 5. Binary classification of skin and non-skin: I) Full HSI cube. II) NDGRI-only. III) SNDI-only. IV) NDGRI + SNDI. V) NDGRI + NDVI. VI) NDVI + SNDI. VII) NDGRI + NDVI + SNDI.

Accuracy results for Subject-1 are shown in Table 4. NDGRI had the highest accuracy results. However, when all three indices were combined, we can see in the classification maps that the number of false alarms decreased causing some of the facial features to become much clearer. In addition, one may observe a person in the background of Subject 1 image next to his left ear. Although this person's facial features are not clear his presence is clearly visible in NDGRI's pseudo color composition, the RGB composite, and in multiple binary classifications.

The second image corresponds to Subject-4 data. Subject 4's experimental conditions were different from Subject 1. Subject-4 was placed in a grassy area sitting down next to a 99% white standard. This is a more complex scene. The white standard was placed in the scene to help in the calibration of the image to reflectance units. The calibrated image was generated by averaging the spectral responses over the white standard and dividing all of the pixels in the image by that average response. Figure 6 displays a summary of the results for Subject-4. Table 5 summarizes the corresponding accuracy assessment.

Downloaded From: http://proceedings.spiedigitallibrary.org/ on 05/30/2015 Terms of Use: http://spiedl.org/terms

Table 4. Accuracy assessment for Subject-1 face image.

				NDGRI, NDVI & SNDI	NDGRI & NDVI	NDGRI & SNDI	NDGRI	SNDI	All Bands	NDVI & SNDI
Subject One	Test	non-skin	producer	99.43	99.96	99.33	99.81	93.37	99.00	93.51
			user	98.01	92.45	99.40	99.99	86.30	78.93	83.00
		skin	producer	94.33	77.01	98.32	99.97	58.27	25.62	46.10
			user	98.33	99.86	98.11	99.46	75.74	90.13	71.62
		Total		98.09	93.94	99.06	99.85	84.17	79.76	81.08
	Train	non-skin	producer	99.91	99.99	99.90	99.99	93.21	97.57	94.11
			user	100.00	100.00	100.00	100.00	98.93	99.71	99.07
		skin	producer	100.00	100.00	100.00	99.99	80.88	94.53	83.16
			user	98.31	99.90	98.13	99.90	38.52	67.16	42.60
		Total		99.91	99.99	99.90	99.99	92.59	97.42	93.56

Results for Subject-4 were qualitatively similar to those for Subject-1 in both raw (before calibration) and calibrated images. NDGRI continues to do a good job in highlighting skin by itself in all cases. However, after calibration, the exposed arms become more visible but the number of false alarms also increased as you can see from the classification result. Also, when combining all there indices, the number of false alarms decreased and skin features became clearer in the image. The accuracies reported in Table 5 confirmed that for the most part NDGRI does and excellent discrimination work by itself in the testing and training data. Accuracies may improve a bit when all three indices are combined. However, visual analysis of the classification map shows a significant reduction in false alarms for the three index combinations when compared to the NDGRI classification map. This can be significant as in a search and rescue operation we are reducing the search area by reducing the false alarms.

5. CONCLUSION AND FUTURE WORK

This paper presented some preliminary results in skin detection using hyperspectral imagery. The existing NDGRI index does an excellent work by itself in discrimination between skin and non-skin classes. Accuracies in the testing and training data were similar between classifications using the NDGRI by itself and when the NDGRI is combined with the proposed SNDI and the NDVI. However, visual results from the classification maps for the entire image show that false alarms were significantly reduced when the three features were combined over detection using only the NDGRI. This is an important result since our objective is to use the indices to identify regions of interest high probability of detection should be accompanied by a low probability of false alarms. The experimental results show that the proposed feature combination of NDGRI+NDVI+SNDI has comparable detection rates with NDGRI by itself but much lower false alarm rates. This is an encouraging result which shows that future work should be pursued.

ACKNOWLEDGEMENTS

Ms. Sanchez was supported by the UTEP NSF-STEM Scholarship Program (NSF Grant 10-60-113), the 2014 UTEP Provost's Summer Research Assistant Program, the UTEP Texas Instruments Foundation Scholarship Program for Graduate Students, and the UTEP ECE Department. Any options, findings, and conclusions or recommendations express in this material are those of the authors and do not necessarily reflect the views of NSF.

Downloaded From: http://proceedings.spiedigitallibrary.org/ on 05/30/2015 Terms of Use: http://spiedl.org/terms

In addition thanks to Dr. Ion Marques and Dr. Manuel Graña from Universidad del País Vasco (UPV/EHU) for their support in data collection. The SOC-710VP system was purchased with funds provided by the University of Texas System STARS program.

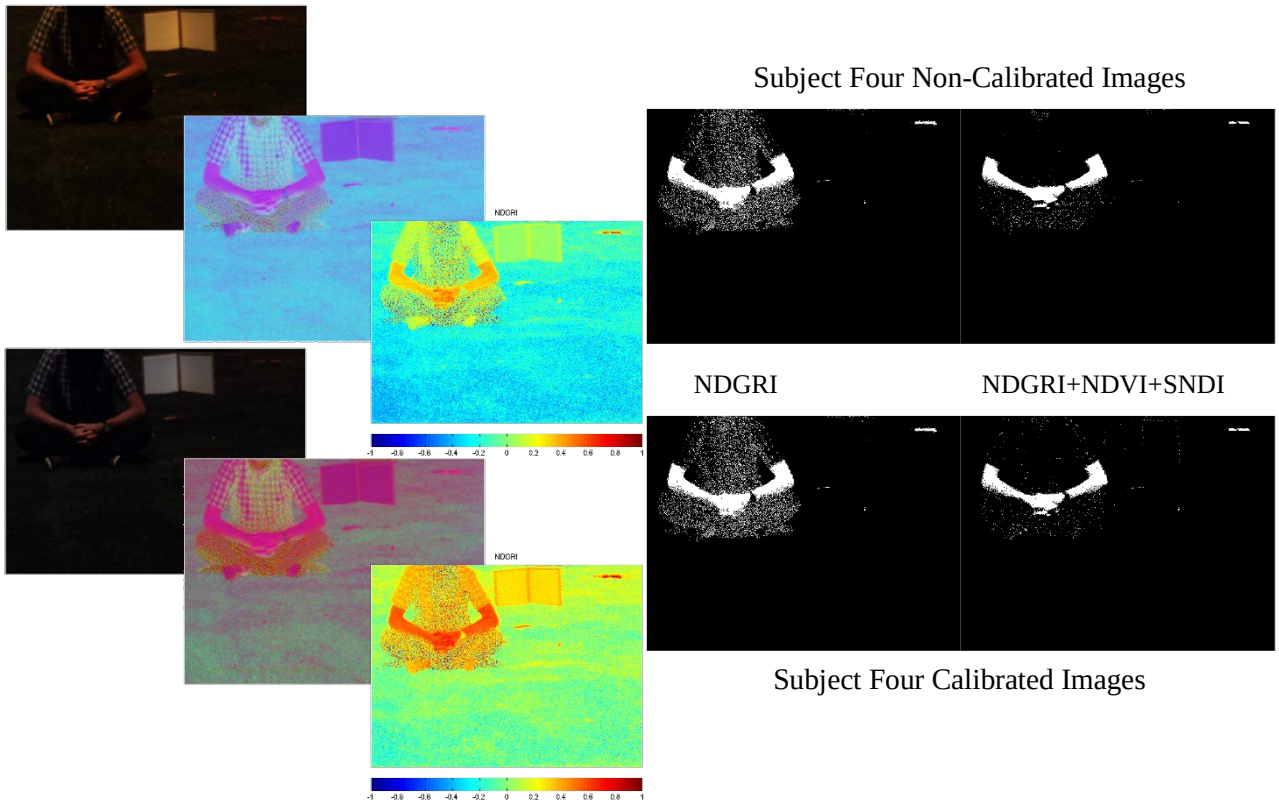

Figure 6. The top three cascade images show an RGB composite before calibration, a 3 band RGB composite of the indices before calibration, and the NDGRI before calibration. The binary images that lie to the right of the cascade show the classification results using the non-calibrated NDGRI and the NDGRI + NDVI + SNDI feature cube. The bottom three cascade images show an RGB composite after calibration, a 3 band RGB composite of the indices after calibration, and the NDGRI after calibration. The binary images that lie to the right show the classification results for the calibrated NDGRI and the NDGRI + NDVI + SNDI feature cube.

REFERENCES

[1] Elgammal, A., Muang, C., and Hu, D., “Skin detection”, Encyclopedia of Biometrics, 1218-1224 (2009).
[2] Eismann, M. T., [Hyperspectral Remote Sensing], SPIE Press, Bellingham, (2012).
[3] Brooks, A.L., [Improved Multispectral Skin Detection and its Applications to Search Space Reduction for Dismount Detection Based on Histograms of Oriented Gradients (Master Thesis)], Air Force Institute of Technology, Wright-Patterson AFB, (2010).
[4] Nunez, A.S., Mendenhall, M.J., "Detection of Human Skin in Near Infrared Hyperspectral Imagery," Proc 2008 IEEE Geoscience and Remote Sensing Symposium Vol.2, II-621-II-624 (2008).
[5] Nixon, K., Rowe, R., Allen, J., "Novel Spectroscopy-based technology for biometric and liveness verification", Proc. SPIE 5404, 287-295 (2004).
[6] Trierscheid, M., Pellenz, J., Paulus, D., Balthasar, D., "Hyperspectral Imaging or Victim Detection with Rescue Robots," Proc. 2008 IEEE International Workshop on Safety Security and Rescue Robotics, 7-12 (2008).

Downloaded From: http://proceedings.spiedigitallibrary.org/ on 05/30/2015 Terms of Use: http://spiedl.org/terms

[7] Bersha, K. S., [Spectral imaging and analysis of human skin (Doctoral dissertation)], University of Eastern Finland, Joensuu, (2010).
[8] Nunez, A.S., [A Physical Model of Human Skin and Its Application for Search and Rescue (Doctoral dissertation)], Air Force Institute of Technology, Wright-Patterson AFB, (2010).
[9] Rosario-Torres, S., Velez-Reyes, M., Hunt, S.D., Jimenez, L.O., "New Developments and Application of the UPRM MATLAB Hyperspectral Image Analysis Toolbox", Proc. SPIE 6565, (2007).
[10] Schowengerdt, R., [Remote sensing models and methods for image processing (3rd ed.)], Academic Press, Burlington, (2007).
[11] Landgrebe, D. A., [Signal Theory Methods in Multispectral Remote Sensing], John Wiley & Sons, (2003).

Table 5. Accuracy Assessment for Subject-4.

				NDGRI, NDVI& SNDI	NDGRI & NDVI	NDGRI & SNDI	NDGRI	SNDI	All Bands	NDVI & SNDI
Subject Four (Un-Cal)	Test	non-skin	producer	99.81	99.73	99.04	98.57	59.87	99.30	99.93
			user	99.93	99.92	99.97	99.98	95.40	98.46	95.94
		skin	producer	98.53	98.49	99.47	99.51	42.67	69.24	16.09
			user	96.39	94.86	83.91	77.82	5.08	83.32	91.65
		total		99.75	99.67	99.06	98.62	59.05	97.86	95.91
	Train	non-skin	producer	99.91	99.85	99.43	99.00	60.35	100.00	99.80
			user	100.00	100.00	100.00	100.00	99.65	99.99	99.95
		skin	producer	100.00	100.00	100.00	100.00	58.15	98.37	89.67
			user	84.40	77.31	47.06	33.64	0.74	100.00	69.92
		total		99.91	99.85	99.43	99.00	60.34	99.99	99.75
Subject Four (Cal)	Test	non-skin	producer	99.76	99.44	99.11	98.47	65.15	99.24	98.50
			user	99.93	99.99	99.47	99.98	95.41	98.50	96.79
		skin	producer	98.62	99.78	89.60	99.56	37.69	69.91	35.02
			user	95.40	89.91	83.58	76.56	5.16	82.31	54.05
		total		99.71	99.45	98.66	98.52	63.83	97.84	95.46
	Train	non-skin	producer	99.89	99.67	99.71	98.96	65.64	100.00	98.34
			user	100.00	100.00	99.98	100.00	99.64	99.99	99.81
		skin	producer	100.00	100.00	96.74	100.00	53.26	98.37	62.50
			user	82.51	60.73	62.90	32.86	0.78	100.00	16.06
		total		99.89	99.67	99.69	98.97	65.57	99.99	98.16

Downloaded From: http://proceedings.spiedigitallibrary.org/ on 05/30/2015 Terms of Use: http://spiedl.org/terms